# $K^+$ channel types targeted by synthetic OSK1, a toxin from *Orthochirus scrobiculosus* scorpion venom

Stéphanie MOUHAT*, Violeta VISAN†, S. ANANTHAKRISHNAN‡, Heike WULFF‡, Nicolas ANDREOTTI*, Stephan GRISSMER†, Hervé DARBON§, Michel DE WAARD‖ and Jean-Marc SABATIER*¶[1]

*Laboratoire Cellpep S.A., 13-15 Rue Ledru-Rollin, 13015 Marseille, France, †Universität Ulm, Albert Einstein Allee 11, 89081 Ulm, Germany, ‡Department of Medical Pharmacology and Toxicology, University of California, Davis, CA 95616, U.S.A., §AFMB, CNRS UPR 9039, 31 Chemin Joseph Aiguier, 13402 Marseille, France, ‖INSERM U607, CEA, 17 Rue des Martyrs, 38054 Grenoble Cedex 09, France, and ¶CNRS FRE 2738, Boulevard Pierre Dramard, 13916 Marseille Cedex 20, France

OSK1 ($\alpha$-KTx3.7) is a 38-residue toxin cross-linked by three disulphide bridges that was initially isolated from the venom of the Asian scorpion *Orthochirus scrobiculosus*. OSK1 and several structural analogues were produced by solid-phase chemical synthesis, and were tested for lethality in mice and for their efficacy in blocking a series of 14 voltage-gated and $Ca^{2+}$-activated $K^+$ channels *in vitro*. In the present paper, we report that OSK1 is lethal in mice by intracerebroventricular injection, with a $LD_{50}$ (50 % lethal dose) value of 2 $\mu$g/kg. OSK1 blocks $K_v1.1$, $K_v1.2$, $K_v1.3$ channels potently and $K_{Ca}3.1$ channel moderately, with $IC_{50}$ values of 0.6, 5.4, 0.014 and 225 nM respectively. Structural analogues of OSK1, in which we mutated positions 16 ($Glu^{16} \rightarrow Lys$) and/or 20 ($Lys^{20} \rightarrow Asp$) to amino acid residues that are conserved in all other members of the $\alpha$-KTx3 toxin family except OSK1, were also produced and tested. Among the OSK1 analogues, [$K_{16}$,$D_{20}$]-OSK1 (OSK1 with $Glu^{16} \rightarrow Lys$ and $Lys^{20} \rightarrow Asp$ mutations) shows an increased potency on $K_v1.3$ channel, with an $IC_{50}$ value of 0.003 nM, without loss of activity on $K_{Ca}3.1$ channel. These data suggest that OSK1 or [$K_{16}$,$D_{20}$]-OSK1 could serve as leads for the design and production of new immunosuppressive drugs.

Key words: $Ca^{2+}$-activated $K^+$ channel, OSK1, peptide synthesis, scorpion toxin, voltage-gated $K^+$ channel.

## INTRODUCTION

OSK1 is a toxin initially purified from the venom of the central Asian scorpion *Orthochirus scrobiculosus* [1]. It is a 38-residue peptide cross-linked by three disulphide bridges that are organized according to the conventional pattern of the three-disulphide-bridged scorpion toxins (i.e. C1–C4, C2–C5 and C3–C6) [1,2]. The 3D (three-dimensional) structure of natural OSK1 in solution, determined by $^1$H-NMR [1], shows that the toxin adopts the $\alpha/\beta$ scaffold (i.e. an $\alpha$-helix connected to an antiparallel $\beta$-sheet by two disulphide bridges) common to most characterized scorpion toxins, independent of their size and selectivity towards the various ion channels [3]. Together with KTx1 (kaliotoxin 1) [4], AgTx1–3 (agitoxin 1–3) [5] and BmKTx (*Buthus martensi* kaliotoxin) [6], OSK1 belongs to a structural class referred to as $\alpha$-KTx3 toxins that share between 68 and 90 % sequence identity with each other [7]. According to this nomenclature, OSK1 has been termed $\alpha$-KTx3.7 [8]. OSK1 has been described previously to block apamin-insensitive small-conductance $Ca^{2+}$-activated channels in neuroblastoma-glioma NG108-15 hybrid cells [9], which are most likely to be identical with $K_{Ca}3.1$ channel. Although the solution structure of OSK1 has been solved [1] (Protein Data Bank code 1SCO), characterization of its pharmacological properties still remained poor. In the present paper, we describe the chemical production and characterization of OSK1. The synthetic product was verified to be indistinguishable from natural OSK1 using two-dimensional $^1$H-NMR, and an extensive analysis of its pharmacological profile was achieved, demonstrating that it behaves *in vitro* as a potent inhibitor of a large array of $K^+$ channel subtypes. Structural analogues of OSK1, in which we introduced selective mutations of amino acid residues that are conserved in all members of the $\alpha$-KTx3 toxin family, except OSK1, were also produced and tested for their pharmacology on various $K^+$ channel types.

## EXPERIMENTAL

### Materials

Fmoc ($N^{\alpha}$-fluoren-9-ylmethyloxycarbonyl)–L-amino acids and reagents used for peptide synthesis were obtained from PerkinElmer (Shelton, CT, U.S.A.). Fmoc–Lys(*t*-butyloxycarbonyl)-2-chlorotrityl resin was purchased from Advanced ChemTech (Cambridge, U.K.). Solvents were analytical grade products from SDS (Peypin, France).

### Chemical synthesis and characterization of OSK1 and related analogues

OSK1, [$K_{16}$]-OSK1, [$D_{20}$]-OSK1, [$K_{16}$,$D_{20}$]-OSK1, [$P_{12}$,$K_{16}$,$D_{20}$]-OSK1 and [$K_{16}$,$D_{20}$,$Y_{36}$]-OSK1 (where $P_{12}$ is an $Arg^{12} \rightarrow Pro$ mutation, $K_{16}$ is a $Glu^{16} \rightarrow Lys$ mutation, $D_{20}$ is a $Lys^{20} \rightarrow Asp$ mutation and $Y_{36}$ is a $Thr^{36} \rightarrow Tyr$ mutation) were all produced by chemical solid-phase synthesis using an automated peptide synthesizer (Model 433A, Applied Biosystems Inc.). In all cases, peptide chains were assembled stepwise on 0.40 mmol of

Abbreviations used: AgTx, agitoxin; $[Ca^{2+}]_i$, internal $Ca^{2+}$ concentration; FCS, foetal calf serum; Fmoc, $N^{\alpha}$-fluoren-9-ylmethyloxycarbonyl; GFP, green fluorescent protein; $K_{Ca}2.1$, $K_{Ca}2.2$ and $K_{Ca}2.3$ channels, type 1, 2 and 3 small-conductance $Ca^{2+}$-activated $K^+$ channels (SK1, SK2 and SK3 respectively); $K_{Ca}3.1$ channel, type 1 intermediate-conductance $Ca^{2+}$-activated $K^+$ channel (IK1); $K_{Ca}1.1$ channel, large-conductance $Ca^{2+}$-activated $K^+$ channel (BK or Slo$\alpha$); $K_v$ channel, mammalian voltage-gated $K^+$ channel; $K_v11.x$ channel, human *ether-a-go-go*-related $K^+$ channel (HERG); KTx1, kaliotoxin 1; $LD_{50}$, 50 % lethal dose; MALDI–TOF, matrix-assisted laser-desorption ionization–time-of-flight; NOE, nuclear Overhauser effect; OSK1, toxin 1 from the scorpion *Orthochirus scrobiculosus* ($\alpha$-KTx3.7); *t*-Bu, *t*-butyl; TFA, trifluoroacetic acid; 3D, three-dimensional.

[1] To whom correspondence should be addressed (email sabatier.jm@jean-roche.univ-mrs.fr).

Fmoc–Lys(*t*-butyloxycarbonyl)-2-chlorotrityl resin (1 % cross-linked; 0.69 mmol of amino group/g) using 1 mmol of Fmoc–L-amino acid derivatives [10]. The side-chain-protecting groups used for trifunctional residues were: Trt (trityl) for cysteine, asparagine, histidine and glutamine; *t*-Bu (*t*-butyl) for serine, threonine, tyrosine, aspartate and glutamate; Pmc (pentamethylchroman) for arginine; and Boc (*t*-butyloxycarbonyl) for lysine. $N^{\alpha}$-amino groups were deprotected by successively treating with 18 and 20 % (v/v) piperidine/*N*-methylpyrrolidone for 3 and 8 min respectively. After three washes with *N*-methylpyrrolidone, the Fmoc–amino acid derivatives were coupled (20 min) as their hydroxybenzotriazole-active esters in *N*-methylpyrrolidone (2.5-fold excess). After complete assembly of the peptides, and removal of their N-terminal Fmoc groups, the peptide resins (approx. 2.4 g) were treated under stirring for 2.5 h at 25 °C with mixtures of TFA (trifluoroacetic acid)/water/thioanisole/ethanedithiol (88:5:5:2, by vol.) in the presence of crystalline phenol (2.25 g) in final volumes of 30 ml/g of peptide resins. The peptide mixtures were filtered, precipitated and washed twice with cold diethyl oxide. The crude peptides were pelleted by centrifugation (3000 ***g*** for 10 min). The crude peptides were then dissolved in water and freeze-dried. Reduced peptides were solubilized (approx. 0.8 mM) in 0.2 M Tris/HCl buffer, pH 8.3, for oxidative folding (40–140 h, depending on the analogue, 22 °C). All peptides were purified to homogeneity by reversed-phase HPLC (PerkinElmer; $C_{18}$ Aquapore ODS 20 $\mu$m, 250 mm × 10 mm) by means of a 60-min linear gradient of 0.08 % (v/v) TFA/0–35 % acetonitrile in 0.1 % (v/v) TFA/water at a flow rate of 6 ml/min ($\lambda = 230$ nm). The purity and identity of the peptides were assessed by: (i) analytical $C_{18}$ reversed-phase HPLC (Merck; $C_{18}$ Lichrospher 5 $\mu$m, 4 mm × 200 mm) using a 60-min linear gradient of 0.08 % (v/v) TFA/0–60 % acetonitrile in 0.1 % (v/v) TFA/water at a flow rate of 1 ml/min; (ii) Edman sequencing; and (iii) molecular mass determination by MALDI–TOF (matrix-assisted laser-desorption ionization–time-of-flight) MS.

### Conformational analyses of OSK1 by two-dimensional $^1$H-NMR and of its analogues by one-dimensional $^1$H-NMR

Peptides were dissolved in a mixture of $H_2O/^2H_2O$ (9:1, v/v) at final concentrations of $10^{-3}$ M (OSK1) or 50 $\mu$M (OSK1 analogues). All $^1$H-NMR measurements were obtained on a Bruker DRX 500 spectrometer equipped with an HCN probe, and self-shielded triple-axis gradients were used. The experiments were performed at 300 K.

### Neurotoxicity of the peptides in mice

OSK1 and its analogues were tested *in vivo* for toxicity by determining the $LD_{50}$ (50 % lethal dose) after intracerebroventricular injection into 20 g C57/BL6 mice (approved by the French ethics committee; animal testing agreement number 006573 delivered by the National Department 'Santé et Protection Animales, Ministère de l'Agriculture et de la Pêche'). Groups of four to six mice per dose were injected with 5 $\mu$l of peptide solution containing 0.1 % (w/v) BSA and 0.9 % (w/v) NaCl.

### Cells

L929 and MEL (murine erythroleukaemia) cells stably expressing mouse $K_v1.3$ ($mK_v1.3$), human $K_v1.5$ ($hK_v1.5$) and mouse $K_v3.1$ ($mK_v3.1$) channels, and COS-7 cells were maintained in DMEM (Dulbecco's modified Eagle's medium) with Earle's salts (Gibco, Paisley, U.K.) and 10 % (v/v) heat-inactivated FCS (foetal calf serum) (PAA Laboratories, Pasching, Austria) as described previously [11]. The tsA cell line expressing human $K_{Ca}3.1$ ($hK_{Ca}3.1$) channels was a gift from Dr Daniel Devor (University of Pittsburgh, Pittsburgh, PA, U.S.A.) and was maintained in MEM (minimal essential medium) with Earle's salts supplemented with Glutamax-I (Gibco), 10 % heat-inactivated FCS and 200 $\mu$g/ml geneticin (G418). Cells were kept at 37 °C in a humidified incubator containing 5 % (for the L929 cell line expressing $mK_v3.1$ channel) or 10 % $CO_2$ (for the other cell lines).

LTK− cells (lacking leucocyte tyrosine kinase) expressing human $K_v1.4$ ($hK_v1.4$) channel were obtained from Professor Michael Tamkun (Colorado State University, Fort Collins, CO, U.S.A.), CHL (Chinese-hamster lung) cells expressing mouse $K_v1.7$ ($mK_v1.7$) channel were from Vertex Pharmaceuticals (San Diego, CA, U.S.A.), HEK-293 (human embryonic kidney) cells expressing human $K_{Ca}1.1$ (hBK or hSlo$\alpha$) channel were from Dr Andrew Tinker (Centre for Clinical Pharmacology, University College London, London, U.K.), HEK-293 cells expressing $K_v11.x$ [HERG (human *ether-a-go-go*-related gene)] channel were from Professor Craig T. January (Department of Medicine, University of Wisconsin, Madison, WI, U.S.A.), and HEK-293 cells expressing human $K_{Ca}2.1$ ($hK_{Ca}2.1$) and rat $K_{Ca}2.2$ ($rK_{Ca}2.2$) channels were from Dr Khaled Houamed (University of Chicago, Chicago, IL, U.S.A.).

### Transfection

The GFP (green fluorescent protein)-IRES vector (Invitrogen, Heidelberg, Germany) containing the coding sequence of mouse $K_v1.1$ ($mK_v1.1$) channel was transfected into COS-7 cells, while the pcDNA3/Hygro vectors (Invitrogen) containing the coding sequence of human $K_v1.2$ ($hK_v1.2$) channel or human $K_{Ca}2.3$ ($hK_{Ca}2.3$) channel, were co-transfected together with a GFP construct. Currents were measured 1–3 days after transfection. In all cases, FuGene6 Transfection Reagent (Roche, Mannheim, Germany) was used for transfection, according to the recommended protocol.

### Electrophysiological recordings

All experiments were carried out at room temperature (22–25 °C) using the whole-cell recording mode of the patch-clamp technique [12,13]. Cells were bathed with mammalian Ringer's solution containing 160 mM NaCl, 4.5 mM KCl, 2 mM $CaCl_2$, 1 mM $MgCl_2$ and 10 mM Hepes, pH 7.4 (with NaOH), with an osmolarity of 290–320 mOsm. When OSK1 peptides were applied, 0.1 % (w/v) BSA was added to the Ringer's solution. A simple syringe-driven perfusion system was used to exchange the bath solution in the recording chamber. The internal pipette solution used for measuring voltage-gated $K^+$ currents contained 155 mM KF, 2 mM $MgCl_2$, 10 mM EGTA and 10 mM Hepes, pH 7.2 (with KOH), with an osmolarity of 290–320 mOsm. For measuring $K^+$ currents through $K_{Ca}3.1$ and $K_{Ca}2.1$–2.3 channels, an internal pipette solution containing 135 mM potassium aspartate, 8.7 mM $CaCl_2$, 2 mM $MgCl_2$, 10 mM EGTA and 10 mM Hepes, pH 7.2 (with KOH), with an osmolarity of 290–320 mOsm {free $[Ca^{2+}]_i$ (internal calcium concentration) = $10^{-6}$ M}, was used. Currents through $mK_v1.1$, $hK_v1.2$, $hK_v1.4$, $hK_v1.5$, $mK_v1.7$ and $mK_v3.1$ channels were elicited with depolarizing voltage steps from − 80 mV to + 40 mV, for 200 ms applied every 10 s. For recordings from $mK_v1.3$ channel, the same pulse step was applied every 30 s. Currents through $hK_{Ca}3.1$, $hK_{Ca}2.1$, $rK_{Ca}2.2$, $hK_{Ca}2.3$ and $hK_{Ca}1.1$ (hBK or hSlo$\alpha$) channels were elicited by 1 $\mu$M $[Ca^{2+}]_i$. For SK and $K_{Ca}3.1$ channels, a voltage-ramp from − 120 mV to 0 ($K_{Ca}3.1$) or + 40 mV of 400 or 200 ms duration was used, while $K_{Ca}1.1$ currents were recorded with a voltage-ramp from − 100 to + 100 mV (200 ms) applied

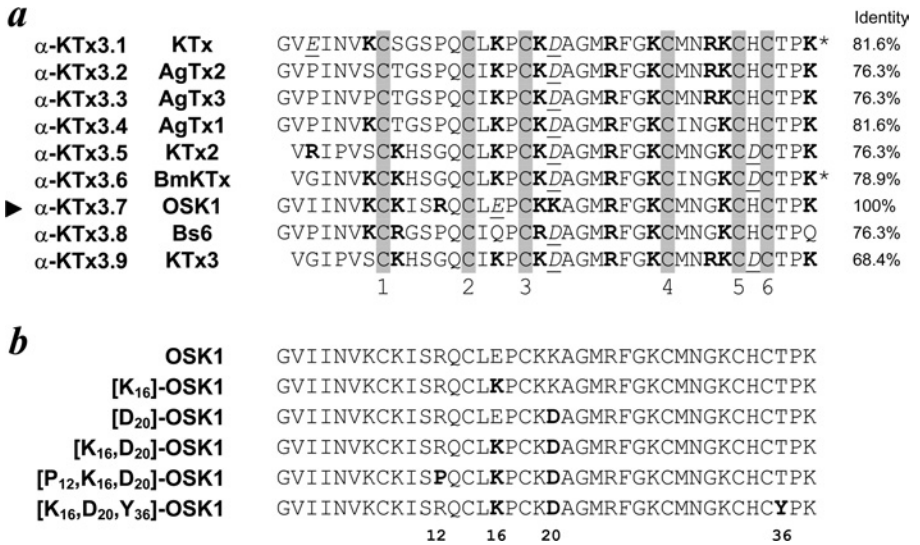


**Figure 1 Amino acid sequence (one-letter code) of OSK1 and comparison with those of other toxins belonging to the α-KTx3 structural family**

(**a**) The amino acid sequences of scorpion toxins were aligned according to the positions of their half-cystine residues, numbered 1–6. The positions of half-cystine residues are highlighted in grey boxes. The asterisk indicates a C-terminal carboxylamidated extremity. Amino acid sequence identities (%) with OSK1 are indicated on the right. The position of OSK1 is indicated by an arrow. Basic and acidic residues are shown in bold and underlined italics, respectively. (**b**) Amino acid sequences of OSK1 and its chemically produced analogues. Mutated residues are shown in bold and numbered. The 3D solution structure of OSK1 can be found in the Protein Data Bank (code 1SCO) [1].

every 10 s. Electrodes were pulled from glass capillaries (Science Products, Hofheim, Germany) in three stages, and fire-polished to resistances measured in the bath of 2.5–5 MΩ. Membrane currents were measured with an EPC-9 or EPC-10 patch-clamp amplifier (HEKA Elektronik, Lambrecht, Germany) interfaced to a Macintosh or PC running acquisition and analysis software (Pulse and PulseFit). When voltage-dependent $K^+$ currents were measured, the capacitive and leak currents were subtracted using the P/10 procedure. Series resistance compensation (> 80 %) was employed if the current exceeded 2 nA. The holding potential in all experiments was − 80 mV. Data analyses were performed with IgorPro (WaveMetrics, Lake Oswego, OR, U.S.A.), and $K_d$ values were deduced by fitting a modified Hill equation to the data $\{X_{toxin}/X_{control} = 1/[1 + ([toxin]/K_d)]$, where X is the peak current (for $K_v$ channels), or the slope of the ramp current, i.e. the conductance, measured between − 100 and − 60 mV (for $hK_{Ca}3.1$ and $hK_{Ca}2.3$ channels) to the normalized data points obtained at more than four different peptide concentrations. This fit indicates that one peptide molecule is sufficient to block the current through the channel. The S.D.s obtained by this fitting routine reflect the uncertainty of the fit.

## RESULTS

### Synthesis of OSK1 and its analogues

An alignment of OSK1 and other members of the α-KTx3 family based on the relative positioning of the half-cystine residues is shown in Figure 1(a). OSK1 displays some interesting structural differences among α-KTx3 toxins. Instead of the basic lysine residue present in all other members of this family, except Bs6, OSK1 possesses an acidic glutamate residue in position 16. In position 20, where all other toxins contain an acidic aspartate residue, OSK1 has a basic lysine residue. Another distinguishing feature of OSK1 is the presence of a basic arginine residue at position 12 instead of an uncharged proline or glycine residue in all other α-KTx3 toxins. Also, similar to all other α-KTx3 toxins, OSK1 exhibits a threonine residue at position 36, where most other several toxin families (α-KTx1, α-KTx2, α-KTx4, α-KTx6 and α-KTx12) display a tyrosine residue. Since the latter residue has often been involved in $K^+$ channel interaction as part of toxin 'functional' dyads [2], we therefore expected that $Thr^{36}$ would influence the pharmacology of OSK1 towards $K^+$ channels. Accordingly, we produced OSK1 chemically and a series of OSK1 analogues to assess the importance of the specific OSK1 residues $Arg^{12}$, $Glu^{16}$, $Lys^{20}$ and $Thr^{36}$ (Figure 1b). All peptides were prepared by solid-phase synthesis using the stepwise Fmoc/*t*-Bu chemistry as described in [14]. In all cases, the amounts of target peptides linked to their resins illustrate yields of peptide assemblies ranging from 70 % to 80 %. Accordingly, crude reduced peptides, obtained after TFA treatment, were found to be relatively homogeneous, as shown for OSK1 synthesis (Figure 2a). The peptides were folded/oxidized under alkaline conditions for 40–120 h (depending on the nature of the molecule), yielding the crude oxidized peptides (see Figure 2b for OSK1). The main oxidized species were purified to > 99 % homogeneity by preparative $C_{18}$ reversed-phase HPLC (Figure 2c for OSK1 is shown as an example). The mass spectrometric analyses of the peptides using the MALDI–TOF technique gave experimental molecular masses that are similar to or identical with the deduced molecular masses (Figure 2d). The yield of each peptide synthesis was approx. 1–3 %. In the case of OSK1, a complete Edman sequencing was also performed to validate its primary structure (results not shown) and check for the presence of standard half-cystine pairings of the type C1–C4, C2–C5 and C3–C6, common to three-disulphide-bridged toxins structured according to an α/β scaffold [1,15].

### Structural analysis of OSK1 and its analogues by $^1$H-NMR

The two-dimensional $^1$H-NMR spectrum of synthetic OSK1 is consistent with a peptide folding according to an α/β scaffold, with evidence for α-helical and β-sheet structures (Figure 3a). These experimental data are consistent with the 3D solution

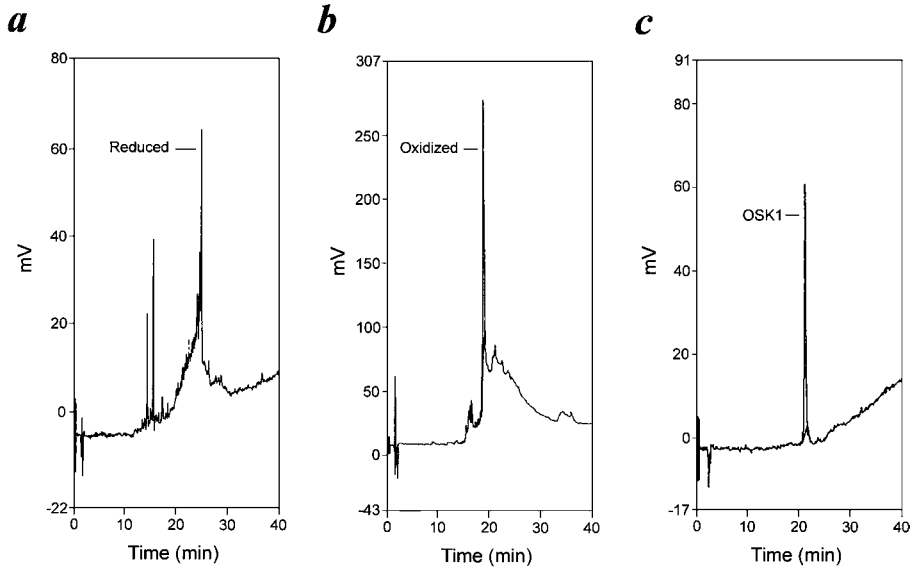


**d**

| Peptide | Deduced Mr $(M+H)^+$ | Experimental Mr $(M+H)^+$ |
|---|---|---|
| OSK1 | 4206.2 | 4206.6 |
| $[K_{16}]$-OSK1 | 4205.3 | 4205.6 |
| $[D_{20}]$-OSK1 | 4193.1 | 4193.1 |
| $[K_{16},D_{20}]$-OSK1 | 4192.2 | 4193.0 |
| $[P_{12},K_{16},D_{20}]$-OSK1 | 4133.1 | 4133.0 |
| $[K_{16},D_{20},Y_{36}]$-OSK1 | 4254.3 | 4254.7 |

**Figure 2 Synthesis and characterization of OSK1 and its analogues**

(**a**) Analytical $C_{18}$ reversed-phase HPLC elution profile of crude reduced OSK1. Note the presence of non-peptide chemical scavengers in the elution profile (elution times approx. 15 min) that later 'disappeared' during oxidative folding, presumably by sticking to the plastic support. (**b**) Elution profile of crude folded/oxidized OSK1 after 72 h oxidation time. (**c**) Elution profile of folded/oxidized OSK1 after purification. (**d**) Deduced and experimental relative molecular masses $(M+H)^+$ of synthetic OSK1 and analogues.

structure of the natural OSK1 solved by $^1$H-NMR [1]. We also used one-dimensional $^1$H-NMR to verify that the mutations introduced in the OSK1 analogues did not alter folding according to the $\alpha/\beta$ scaffold (Figure 3b). Indeed, similar overall distributions of the resonance frequencies of the different peptides indicate that they adopt closely related conformations.

### Lethal activity of OSK1 and its analogues in mice

We determined $LD_{50}$ values for the synthetic peptides by injecting them intracerebroventricular into mice (Table 1). All peptides proved to be lethal in mice with symptoms (tremors, convulsions and spasmic paralysis) resembling those induced by inoculation of $K^+$ channel toxin blockers (S. Mouhat and J.-M. Sabatier, unpublished work). The order of *in vivo* toxicity was OSK1 > $[K_{16},D_{20}]$-OSK1 > $[K_{16}]$-OSK1 > $[D_{20}]$-OSK1 > $[P_{12},K_{16},D_{20}]$-OSK1 > $[K_{16},D_{20},Y_{36}]$-OSK1. The greatest difference observed in $LD_{50}$ values was 4.5-fold between OSK1 and $[K_{16},D_{20},Y_{36}]$-OSK1. The $LD_{50}$ value observed for OSK1 is of the same order as the $LD_{50}$ values observed for other potent $K^+$-channel-acting scorpion toxins [15–17]. Assuming that OSK1 would diffuse immediately throughout the entire mouse brain (40 ng of toxin in 400 $\mu$l of brain volume) following the injection, the toxin concentration in the brain would be approx. 20 nM. Right at the injection site, the toxin might even briefly reach micromolar concentrations. We therefore believe that the convulsions and the lethality of the OSK1 peptides are caused by inhibition of brain $K_v1.1$ and $K_v1.2$ channels (see $IC_{50}$ values for these channels in Table 1 and the following section).

### Pharmacological activity of OSK1 and its analogues on various $K^+$ channels

#### Effects of OSK1

We studied the pharmacological profile of OSK1 on a panel of 14 $K^+$ channels (nine voltage-gated and five $Ca^{2+}$-activated $K^+$ channels). Table 1 illustrates that OSK1 is a highly potent $K_v$ channel blocker. The most remarkable features of OSK1 are: (i) its potency to block $K_v1.3$ channel at picomolar concentrations ($IC_{50}$ value of 14 pM), which classifies it among the best $K_v1.3$ channel blockers (with *Stichodactyla helianthus* sea anemone ShK toxin, and AgTx2 and *Heterometrus spinnifer* HsTx1 scorpion toxins [5,18–20]), and (ii) its ability to block all three $K_v$ channels ($K_v1.1$, $K_v1.2$ and $K_v1.3$) with high potency. The decreasing order of blocking efficacy is $K_v1.3 > K_v1.1 > K_v1.2$ (lower $IC_{50}$ value of 5.4 nM). This ability to block all three $K^+$ channels is unusual, since most toxins characterized so far are either active on $K_v1.2$ or $K_v1.3$ channel alone, or on the combination of $K_v1.1$ and $K_v1.3$ channels [14,15,19–24]. This peculiar behaviour of OSK1 does not stem from a lack of specificity, since the toxin is inactive

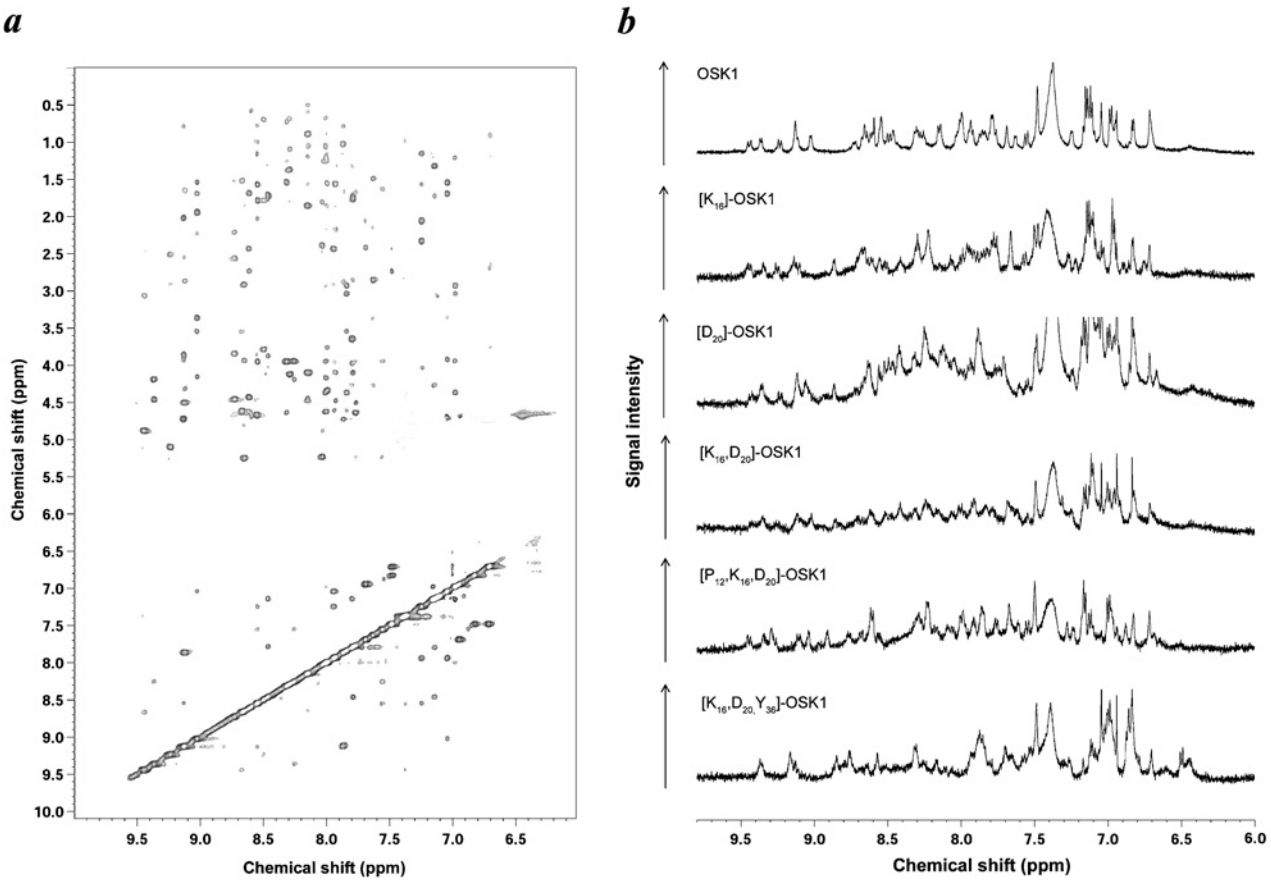


**Figure 3 Structural analysis of OSK1 and its analogues by $^1$H-NMR**

(**a**) Contour plot of a NOESY spectrum of synthetic OSK1. Fingerprint and amide proton regions are shown on top and bottom, respectively. (**b**) One-dimensional $^1$H-NMR spectra of OSK1 and its analogues. Only the representative amide proton regions are shown. Note that the overall distribution of resonance frequencies suggests that the 3D structures of all six peptides are similar.

**Table 1 Bioactivities of OSK1 and its analogues *in vivo* in mice and *in vitro* on 14 different $K^+$ channel types**

$LD_{50}$ values for each toxin are given in parentheses ($\mu$g/kg of mice). See the Experimental section for details. No effect (ne) was seen for any of the peptides on $K_v1.4$, $K_v1.5$, $K_v1.6$, $K_v3.1$, $K_v11.x$, $K_{Ca}2.1$, $K_{Ca}2.2$, $K_{Ca}2.3$ and $K_{Ca}1.1$ channels, indicating a lack of blocking activity at micromolar peptide concentration.

| | $IC_{50}$ (nM) | | | | | |
|---|---|---|---|---|---|---|
| Channel | OSK1 (2) | $[K_{16}]$-OSK1 (3) | $[D_{20}]$-OSK1 (4.5) | $[K_{16},D_{20}]$-OSK1 (2.5) | $[P_{12},K_{16},D_{20}]$-OSK1 (7.5) | $[K_{16},D_{20},Y_{36}]$-OSK1 (9) |
| $K_v1.1$ | $0.60 \pm 0.04$ | $0.63 \pm 0.05$ | $2.95 \pm 0.24$ | $0.40 \pm 0.01$ | $3.18 \pm 0.11$ | $34.4 \pm 0.3$ |
| $K_v1.2$ | $5.40 \pm 1.89$ | $5.23 \pm 0.22$ | $77.8 \pm 9.2$ | $2.96 \pm 0.01$ | $196 \pm 9$ | $232 \pm 11$ |
| $K_v1.3$ | $0.014 \pm 0.001$ | $0.067 \pm 0.006$ | $0.037 \pm 0.007$ | $0.003 \pm 0.001$ | $0.059 \pm 0.003$ | $0.122 \pm 0.007$ |
| $K_v1.7$ | ne | ne | ne | ne | ne | $1500 \pm 500$ |
| $K_{Ca}3.1$ | $225 \pm 10$ | $151 \pm 21$ | $716 \pm 10$ | $228 \pm 92$ | $2600 \pm 400$ | $885 \pm 18$ |

on $K_v1.4$, $K_v1.5$, $K_v1.6$, $K_v1.7$ and $K_v11.x$ channels (Table 1). Also, OSK1 has no effect on $K_{Ca}2.1$, $K_{Ca}2.2$, $K_{Ca}2.3$ and $K_{Ca}1.1$ channels when in the micromolar concentration range, whereas it shows a moderate activity on $K_{Ca}3.1$ channel (also referred to as IK1 or SK4) with an $IC_{50}$ value of 225 nM. Figure 4 summarizes the effects of OSK1 on the channels that are sensitive to this toxin. It illustrates that saturating concentrations of OSK1 induce a complete block of the outward $K^+$ current for each channel type. A comparison of the pharmacological properties of synthetic OSK1 with its natural counterpart was not possible since the latter was not available.

## Effects of OSK1 analogues

We have noticed that OSK1 displays two unusual properties for a member of the $\alpha$-KTx3 family: one structural and one functional. First, some charged amino acid residues differ between OSK1 and other $\alpha$-KTx3 toxins, such as the acidic $Glu^{16}$ and the basic $Lys^{20}$, which are only present in OSK1. At equivalent positions, other toxins have a basic lysine residue and an acidic aspartate residue. One exception to this rule is Bs6 ($\alpha$-KTx3.8; Figure 1) that possesses an uncharged glutamine residue at position 16. Overall, this corresponds to an inversion of charged residues within the

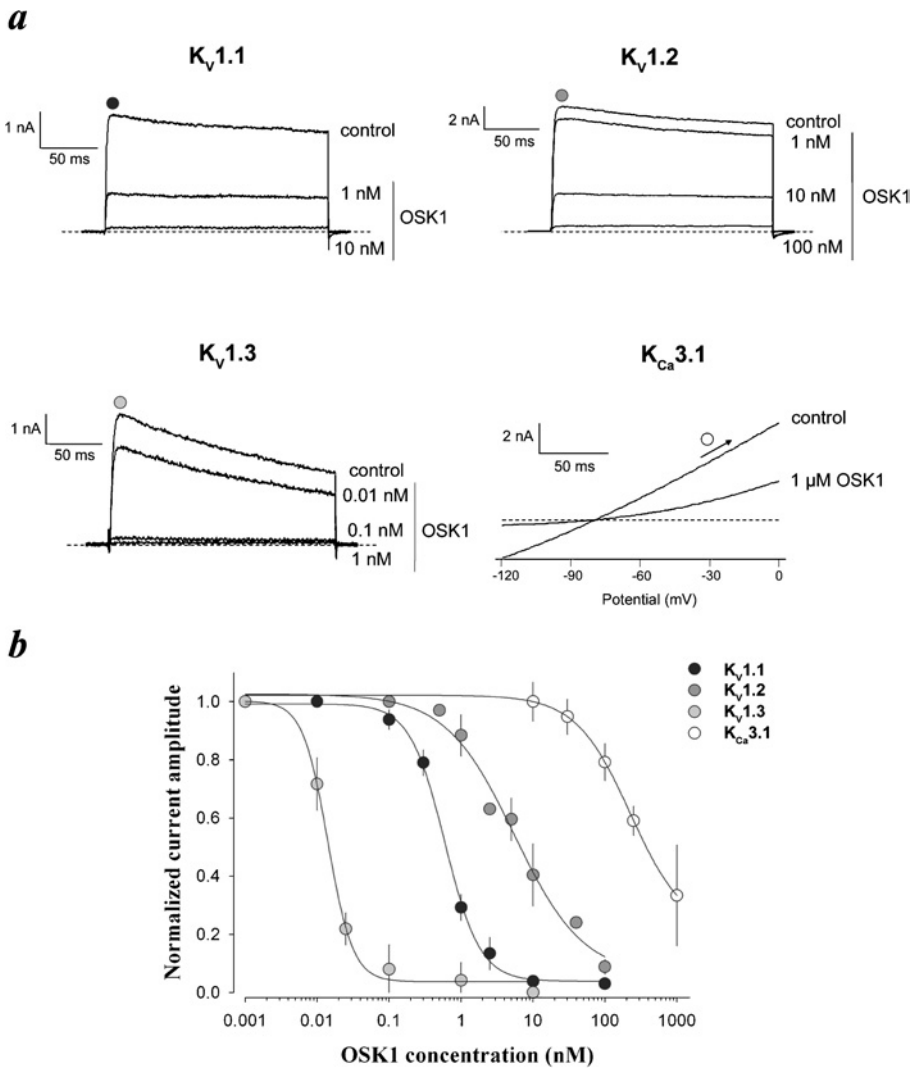


**Figure 4 Block of voltage-gated $K_v1.1$, $K_v1.2$, $K_v1.3$ and $Ca^{2+}$-activated $K_{Ca}3.1$ channels by OSK1**

(**a**) Original current traces in the absence (control) or presence of synthetic OSK1 at various concentrations. Top left, block of $K_v1.1$ current by OSK1. Top right, block of $K_v1.2$ current. Bottom left, block of $K_v1.3$ current. For each $K_v$-channel type, currents were elicited by depolarizing voltage steps from the holding potential $-80$ mV to $+40$ mV for 200 ms. Bottom right, OSK1-induced block of $K_{Ca}3.1$ current. Currents were elicited by 1 $\mu$M $[Ca^{2+}]_i$ and voltage ramps from the holding potential $-80$ mV to $+40$ mV for 400 ms. (**b**) Average normalized current inhibition by various concentrations of OSK1 for each channel type. Results are means $\pm$ S.D. ($n = 4$–5).

OSK1 primary structure. Secondly, OSK1 has an unexpected wide range of activity, i.e. on $K_v1.1$, $K_v1.2$ and $K_v1.3$ channels, a property usually not shared by other toxins from this structural family. We therefore speculated that these two properties might be connected and decided to evaluate the pharmacological impact of restoring the more conventional amino acid residues at relevant positions within the OSK1 sequence ($Lys^{16}$ instead of $Glu^{16}$, and $Asp^{20}$ instead of $Lys^{20}$). First, we investigated the effects of mono-substitutions: $[K_{16}]$-OSK1 and $[D_{20}]$-OSK1 (Table 1). For $[K_{16}]$-OSK1, only slight differences in the pharmacological profile were observed, except the $K_v1.3$ channel, for which a 4.8-fold decrease in blocking efficacy was found ($IC_{50}$ value of 67 pM instead of 14 pM). For $[D_{20}]$-OSK1, more pronounced effects were observed, with decreased blocking efficacy ranging from 2.5- to 14-fold depending on the ion channel type under consideration (Table 1). Thus both amino acid residues of OSK1 appear to contribute to differences in toxin selectivity for $K_v$ channels. In the case of OSK1, there is a 385-fold difference in blocking efficacy between $K_v1.2$ and $K_v1.3$ channels, which is decreased to 78-fold for $[K_{16}]$-OSK1, and increased to 2102-fold for $[D_{20}]$-OSK1. The two substitutions therefore generated somehow opposite effects in altering toxin selectivity towards $K_v$ channels. We investigated further the potential effects of the double substitution on OSK1 pharmacology. We observed that $[K_{16},D_{20}]$-OSK1 annulled both tendencies observed with $[K_{16}]$-OSK1 and $[D_{20}]$-OSK1, taken individually, such that the pharmacological properties of $[K_{16},D_{20}]$-OSK1 and OSK1 resembled each other quite closely. However, the blocking efficacy of $[K_{16},D_{20}]$-OSK1 is increased 1.5-, 1.8- and 4.5-fold on $K_v1.1$, $K_v1.2$ and $K_v1.3$ channels respectively. The difference in blocking efficacy toward $K_v1.2$ and $K_v1.3$ channels is 962-fold, getting closer to what was observed for OSK1, but underlining the greater impact of $Asp^{20}$ substitution. Importantly, this double substitution generated an OSK1 analogue that is extremely potent on $K_v1.3$ channel, with an $IC_{50}$ value of 3 pM

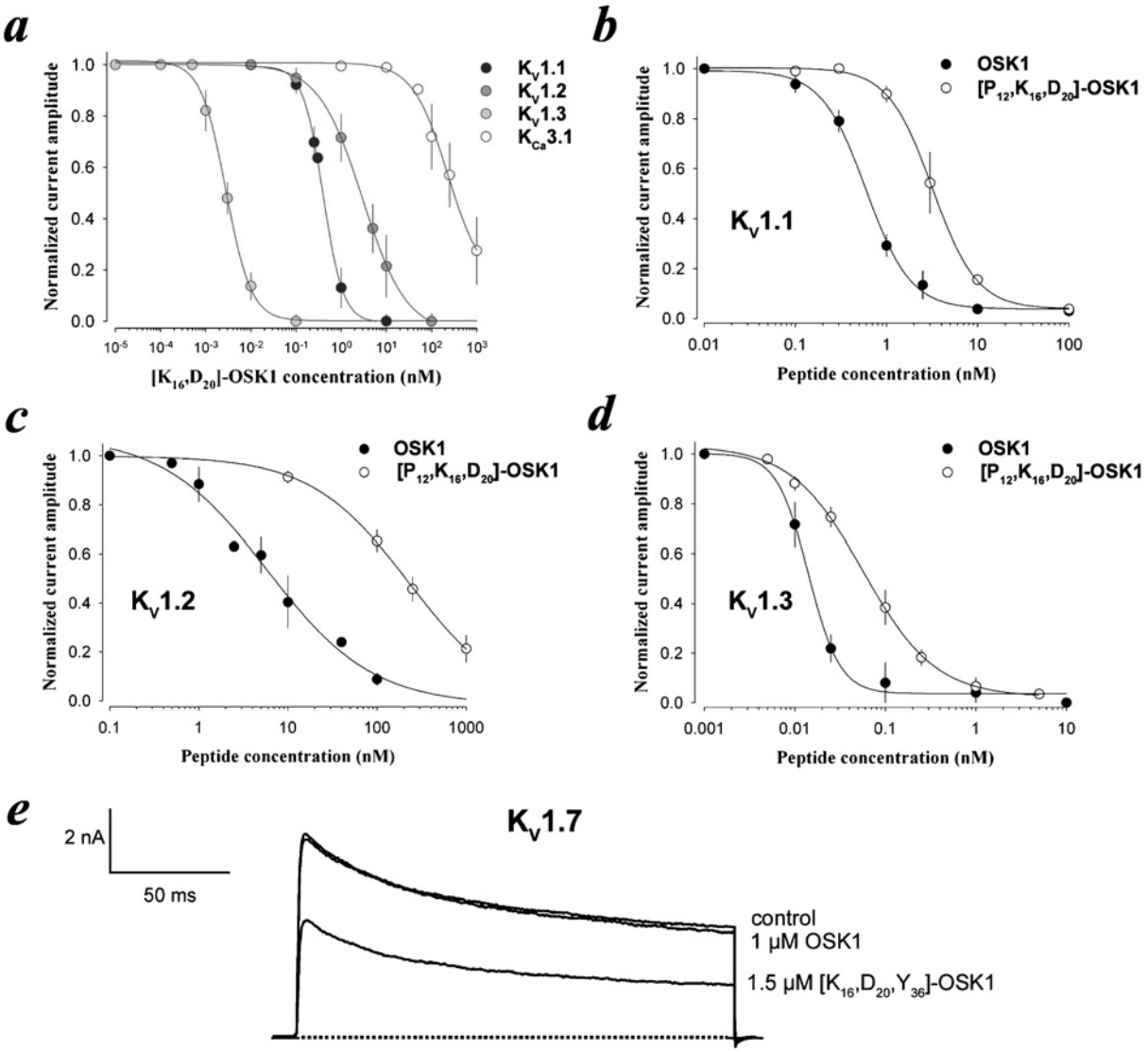


**Figure 5 Activity of OSK1 analogues on $K_v$ channels**

(**a**) Average normalized inhibition of $K_v1.1$, $K_v1.2$, $K_v1.3$ and $K_{Ca}3.1$ currents by various concentrations of $[K_{16},D_{20}]$-OSK1. Each data point corresponds to the mean ± S.D. ($n = 4$–5). (**b**) Average normalized inhibition of $K_v1.1$ currents by various concentrations of $[P_{12},K_{16},D_{20}]$-OSK1 ($n = 5$) and comparison with OSK1 ($n = 5$). (**c**) Average normalized inhibition of $K_v1.2$ currents by various concentrations of $[P_{12},K_{16},D_{20}]$-OSK1 ($n = 3$). (**d**) Average normalized inhibition of $K_v1.3$ currents by various concentrations of $[P_{12},K_{16},D_{20}]$-OSK1 ($n = 5$). (**e**) Current traces elicited at + 40 mV for control condition or after application of 1 $\mu$M OSK1 ($n = 4$) or 1.5 $\mu$M $[K_{16},D_{20},Y_{36}]$-OSK1 ($n = 5$).

(Figure 5a). This value is similar [5] or even better [19,20] than those reported for the best $K_v1.3$ channel blockers described hitherto.

Into this most active analogue, we introduced additional substitutions with the aim of determining their impact on OSK1 pharmacology (Figure 1b). First, we replaced $Arg^{12}$ of $[K_{16},D_{20}]$-OSK1 by a proline residue. The resulting $[P_{12},K_{16},D_{20}]$-OSK1 analogue has decreased activity towards all $K^+$ channels tested by factors ranging from 8- to 66-fold as compared with $[K_{16},D_{20}]$-OSK1, and from 4- to 36-fold as compared with OSK1 (Figures 5b–5d). Although decreased blocking efficacy is generally not a sought-after property for analogues, it should be noticed that $[P_{12},K_{16},D_{20}]$-OSK1's potency towards $K_v1.3$ channel remains high ($IC_{50}$ value of 59 pM), and that the difference in blocking efficacy between $K_v1.2$ and $K_v1.3$ channels is increased to 3322-fold. Altogether, these results suggest the importance of $Arg^{12}$ for OSK1 pharmacology. However, the pharmacological impact of the substitution may be due to either the lack of $Arg^{12}$ in toxin sequence or a change of peptide conformation induced by $Pro^{12}$. Next, we investigated the effect of replacing $Thr^{36}$ by a tyrosine residue that is found in a homologous position in a number of $K_v$-channel-acting scorpion toxins from other $\alpha$-KTx families (Figure 1). This supplemental mutation in $[K_{16},D_{20}]$-OSK1 results in a marked decrease of peptide blocking efficacy towards $K_v1.1$, $K_v1.2$ and $K_v1.3$ channels (from 3.9- to 86-fold, and from 8.7- to 57-fold, as compared with OSK1). Interestingly, we found that $[K_{16},D_{20},Y_{36}]$-OSK1 is significantly active towards $K_v1.7$ channel [25] (Figure 5e), albeit with low potency ($IC_{50}$ value of 1.5 $\mu$M). It is worth noting that none of the other analogues had gained a novel activity so far towards a previously unblocked channel type. Such a channel blockage is of interest, since there is no known inhibitor of this channel type. Future experiments will aim at improving peptide affinity for $K_v1.7$ channel.

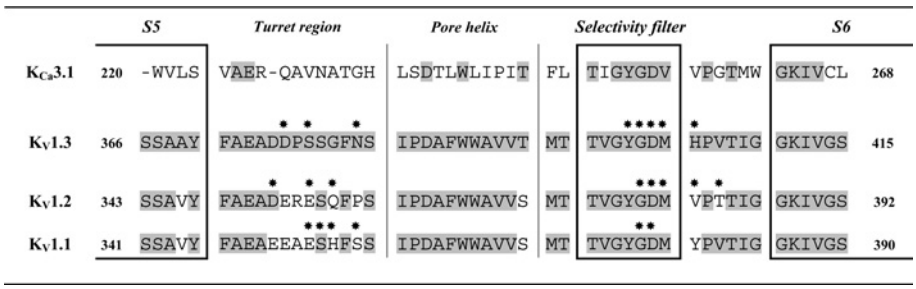


**Figure 6 Comparison of amino acid sequences of pore domains of $K_v$1.3 with $K_v$1.1, $K_v$1.2 and $K_{Ca}$3.1 channels**

Each $K^+$ channel amino acid sequence is numbered and subdivided into structural and/or functional regions (transmembrane segments S5 and S6, turret region, pore helix and selectivity filter). Amino acid sequence identity with $K_v$1.3 channel is shaded grey. Amino acid residues predicted to interact with OSK1 are denoted by asterisks.

## DISCUSSION

Although the 3D structure of OSK1 in solution was solved a few years ago [1], its pharmacological properties remained to be established. In the present study, for the first time, we have produced synthetic OSK1, along with several structural analogues, and have investigated their biological activities extensively on a wide range of potential $K^+$ channel targets. OSK1 is a potent blocker of three different $K_v$ channel types ($K_v$1.1, $K_v$1.2 and $K_v$1.3) and a moderate blocker of $Ca^{2+}$-activated $K_{Ca}$3.1 channel. Of interest, OSK1 is one of the most powerful $K_v$1.3 channel blockers so far described, making it an interesting lead compound for the development of new drugs for the therapy of autoimmune disorders [18,26–29]. A first step in this direction was taken with the production of [$P_{12}$,$K_{16}$,$D_{20}$]-OSK1, which still shows a high affinity, but an improved selectivity for $K_v$1.3 channel. Also, [$K_{16}$,$D_{20}$]-OSK1 exhibits an increased activity towards $K_v$1.3 channel ($IC_{50}$ value of 3 pM with approx. 100 % of current block) compared with OSK1, which places it among the most potent $K_v$1.3 channel blockers reported so far [18]. Therefore [$K_{16}$,$D_{20}$]-OSK1 (or its derivatives) might be of particular value for the management of memory-T-cell-mediated immune responses, such as multiple sclerosis [18,29].

In addition, $K_v$1.3 and $K_{Ca}$3.1 channels have been shown to critically contribute to lymphocyte activation [18,30]. However, the contribution level of each channel type to lymphocyte $K^+$ current is different, depending on the type of activated lymphocytes. $K_v$1.3 current is predominant in effector memory lymphocytes, whereas $K_{Ca}$3.1 current predominates in central memory lymphocytes. An ideal immunomodulatory compound is expected to possess two main properties. First, it should preferentially block either $K_v$1.3 or $K_{Ca}$3.1 channel in order to target one specific subset of T-cells [18]. Secondly, it should be selective for one of these channel types, thus without affecting other $K_v$-variants, in order to avoid unwanted secondary effects. OSK1 presents the first desired property, since it targets $K_v$1.3 channel with a greater potency than $K_{Ca}$3.1 channel. Also, its lower efficacy on other $K_v$-type channels, namely the neuronal variants $K_v$1.1 and $K_v$1.2 channels, is a first asset towards the design of an adequate immunosuppressive drug. Designing of improved compounds is possible since several OSK1 analogues already display increased selectivity for $K_v$1.3 channel. It is worth mentioning that OSK1 thus now belongs to an enlarged family of potent $K_v$1.3 ($\alpha$-KTx 1.1, 2.2, 3.2 and 7.1) and/or $K_{Ca}$3.1 ($\alpha$-KTx 1.1 and 6.2) channel immunosuppressive drugs [31,32]. Forthcoming OSK1-derived analogues will be designed to maintain a high potency on $K_v$1.3 channel and a diminished activity towards other $K_v$-channels.

To gain insight in the differences of OSK1 affinity for the various $K^+$ channels on which this toxin is active, we first compared the amino acid sequences of the pore regions of $K_{Ca}$3.1, $K_v$1.1, $K_v$1.2 and $K_v$1.3 channels with a particular emphasis on the last channel type (Figure 6). Noteworthily, $K_v$-type channels mainly differ in the turret region, whereas amino acid sequence differences with $K_{Ca}$3.1 channel relies further on the pore helix region. Therefore differences in selectivity may preferentially be attributed to specific interactions of toxin residues with these two regions. In particular, a cluster of acidic residues can be observed in the turret region of $K_v$-type channels, which is not the case in $K_{Ca}$3.1 channel. We set out to determine the functional maps of OSK1 on $K_v$1.1, $K_v$1.2 and $K_v$1.3 channels using docking simulations (Figure 7). Of note, the functional map of OSK1 for $K_{Ca}$3.1 channel could not be formally determined owing to its weak docking energy. According to these functional maps, the channel residues involved in an interaction with OSK1 are highlighted by asterisks (Figure 6). Amino acid residues of the various $K_v$ channels that interact with OSK1 appear to be mainly located in the turret region and in or nearby the selectivity filter. A particular focus on $K_v$1.3 channel, which is the channel most sensitive to OSK1, reveals the implication of $Asp^{376}$, $Ser^{378}$, $Asn^{382}$, $Tyr^{400}$, $Gly^{401}$, $Asp^{402}$, $Met^{403}$ and $His^{404}$ residues. Of note, $His^{404}$ behaves as a pivotal residue, since it inhibits the effect of $\alpha$-KTx6.2 (maurotoxin) on $K_v$1.3 channel [33].

Computational simulations (based on Brownian dynamics) with six other toxins, also highly potent on $K_v$1.3 channel, reveal a slightly distinct pattern of molecular interactions [34]. In particular, two channel residues ($Gly^{380}$ and $Asp^{386}$) were predicted to participate in the interaction with these toxins unlike with OSK1. This suggests that OSK1 has a different docking position over $K_v$1.3 channel from those of other $K_v$1.3-channel-acting toxins. Importantly, none of the amino acid residues ($Arg^{12}$, $Glu^{16}$, $Lys^{20}$ and $Thr^{36}$) that were mutated to produce the OSK1 analogues are directly implicated in binding to $K_v$-type channels. For most of these residues ($Arg^{12}$, $Glu^{16}$ and $Lys^{20}$), this was expected, since they belong to the toxin helical structure. Nevertheless, mutating these amino acid residues presumably alters the structure of OSK1, since the docking of [$K_{16}$,$D_{20}$]-OSK1 presents a slightly different pattern of molecular contacts, although the same toxin residues are concerned. In particular, [$K_{16}$,$D_{20}$]-OSK1 now also interacts with $Gly^{380}$, similar to other $K_v$1.3-channel-blocking toxins, but different from OSK1 [34]. Globally, these changes in receptor–ligand contacts may be responsible for the increased affinity of [$K_{16}$,$D_{20}$]-OSK1 for $K_v$-type channels (especially $K_v$1.3) over OSK1. In that respect, $Gly^{380}$ may be one of the contributors of this increased affinity, since it is present in $K_v$1.3, but not in $K_v$1.1 or $K_v$1.2, channel.

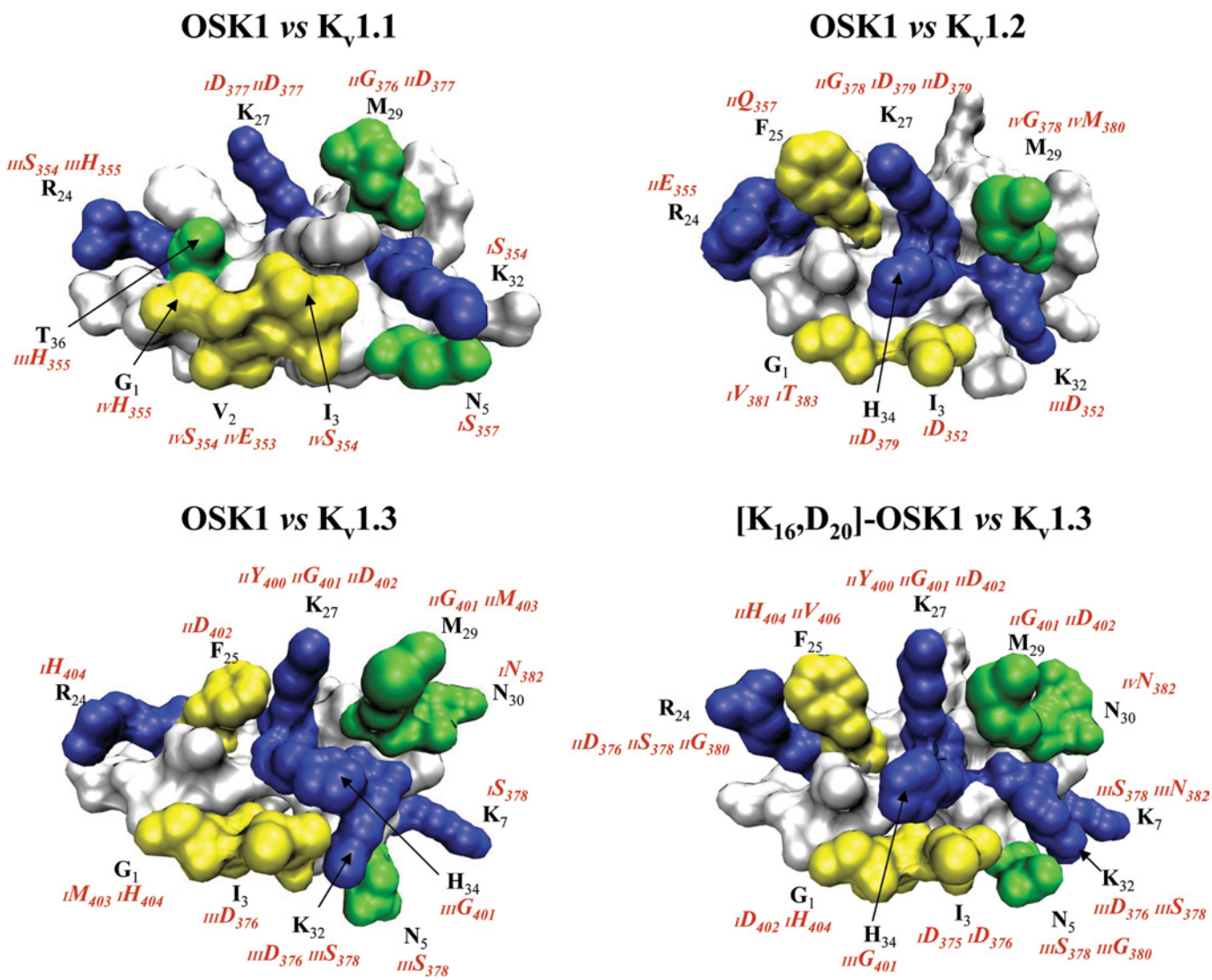


**Figure 7 Functional maps of OSK1 on to $K_v$1.1, $K_v$1.2 and $K_v$1.3, and of [$K_{16}$,$D_{20}$]-OSK1 on to $K_v$1.3 channels**

Theoretical functional maps of OSK1 and [$K_{16}$,$D_{20}$]-OSK1 depicting amino acid residues that are key for peptide interaction with $K_v$1.1, $K_v$1.2 or $K_v$1.3 channels. Interacting residues from the $K_v$ channel are highlighted in red. I to IV before channel residue numbering specifies one of the four $\alpha$-subunits forming a functional $K_v$ channel. Colour codes: yellow (hydrophobic residues), light green (polar residues) and blue (basic residues). These maps were generated by docking simulations [37]. Swiss-Prot accession codes used are P16388 (mouse $K_v$1.1 channel), P16389 (human $K_v$1.2 channel) and P16390 (mouse $K_v$1.3 channel).

Although the docking simulation of OSK1 on the $K_{Ca}$3.1 channel was not reliable, there are interesting parallels to draw from the comparative effects of other toxins on both $K_v$1.3 and $K_{Ca}$3.1 channel. Maurotoxin is highly active on $K_{Ca}$3.1 channel, but is weakly active on $K_v$1.3 channel [35]. Conversely, OSK1 is weakly active on $K_{Ca}$3.1 channel, but is highly potent on $K_v$1.3 channel. Thus a comparison of the functional maps of both toxins should provide some insights into the key molecular determinants that drive these differences in channel selectivity. All functional maps are not available, but a few elements help to identify these molecular determinants. We have noticed that Kv1.3 and $K_{Ca}$3.1 channels differ mainly in the turret and pore helix regions. However, since docking simulation of OSK1 on to $K_v$1.3 channel highlights a number of close contacts only in the turret region, this suggests that the latter region may underlie the difference in OSK1 affinity for $K_v$1.3 and $K_{Ca}$3.1 channels. In agreement with this hypothesis was the finding that mutating $Lys^{32}$ of $\alpha$-KTx1.1 (charybdotoxin), a residue which interacts with $Asp^{376}$ of the $K_v$1.3 channel turret region, strongly decreased toxin affinity for $K_v$1.3 channel without altering affinity for $K_{Ca}$3.1 channel [36]. An equivalent lysine residue is present in OSK1 ($Lys^{32}$), which interacts with $Asp^{376}$ from $K_v$1.3 channel. We thus expect that the higher affinity of OSK1 for $K_v$1.3 over $K_{Ca}$3.1 channel is also partly due to this interaction in the turret region. Although helpful, structural considerations from docking simulations are theoretical, and further experimental validation through targeted point mutations will be needed to confirm the functional importance of the turret region in underlying differences in toxin selectivity.

We thank Dr P. Mansuelle for Edman sequencing and amino acid analysis of OSK1 peptides, and Mr D. Homerick for excellent technical assistance. Dr B. De Rougé and Dr E. Béraud are acknowledged for helpful discussions. This work was supported by funds from Cellpep S.A. (Paris, France).

## REFERENCES


1 Jaravine, V. A., Nolde, D. E., Reibarkh, M. J., Korolkova, Y. V., Kozlov, S. A., Pluzhnikov, K. A., Grishin, E. V. and Arseniev, A. S. (1997) Three-dimensional structure of toxin from *Orthochirus scrobiculosus* scorpion venom. Biochemistry **36**, 1223–1232

2 Mouhat, S., Jouirou, B., Mosbah, A., De Waard, M. and Sabatier, J. M. (2004) Diversity of folds in animal toxins acting on ion channels. Biochem. J. **378**, 717–726

3 Bontems, F., Roumestand, C., Gilquin, B., Ménez, A. and Toma, F. (1991) Refined structure of charybdotoxin: common motifs in scorpion toxins and insect defensins. Science **254**, 1521–1523

4 Aiyar, J., Withka, J. M., Rizzi, J. P., Singleton, D. H., Andrews, G. C., Lin, W., Boyd, J., Hanson, D. C., Simon, M., Dethlefs, B. et al. (1995) Topology of the pore-region of a $K^+$ channel revealed by the NMR-derived structures of scorpion toxins. Neuron **15**, 1169–1181

5 Garcia, M. L., Garcia-Calvo, M., Hidalgo, P., Lee, A. and MacKinnon, R. (1994) Purification and characterization of three inhibitors of voltage-dependent $K^+$ channels from *Leiurus quinquestriatus* var. *hebraeus* venom. Biochemistry **33**, 6834–6839

6 Romi-Lebrun, R., Lebrun, B., Martin-Eauclaire, M.-F., Ishiguro, M., Escoubas, P., Wu, F. Q., Hisada, M., Pongs, O. and Nakajima, T. (1997) Purification, characterization, and synthesis of three novel toxins from the Chinese scorpion *Buthus martensi*, which act on $K^+$ channels. Biochemistry **36**, 13473–13482

7 Tytgat, J., Chandy, K. G., Garcia, M. L., Gutman, G. A., Martin-Eauclaire, M.-F., van der Walt, J. J. and Possani, L. D. (1999) A unified nomenclature for short-chain peptides isolated from scorpion venoms: $\alpha$-KTx. Trends Physiol. Sci. **20**, 444–447

8 Rodriguez de la Vega, R. C. and Possani, L. D. (2004) Current views on scorpion toxins specific for $K^+$ channels. Toxicon **43**, 865–875

9 Grishin, E. V., Korolkova, Y. V., Kozlov, S. A., Lipkin, A. V., Nosyreva, E. D., Pluzhnikov, K. A., Sukhanov, S. V. and Volkova, T. M. (1996) Structure and function of the potassium channel inhibitor from black scorpion venom. Pure Appl. Chem. **68**, 2105–2109

10 Merrifield, R. B. (1986) Solid phase synthesis. Science **232**, 341–347

11 Grissmer, S., Nguyen, A. N., Aiyar, J., Hanson, D. C., Mather, R. J., Gutman, G. A., Karmilowicz, M. J., Auperin, A. A. and Chandy, K. G. (1994) Pharmacological characterization of five cloned voltage-gated $K^+$ channels, types $K_v$ 1.1, 1.2, 1.3, 1.5 and 3.1, stably expressed in mammalian cell lines. Mol. Pharmacol. **45**, 1227–1234

12 Hamill, O. P., Marty, A., Neher, E., Sakmann, B. and Sigworth, F. J. (1981) Improved patch-clamp techniques for high-resolution current recording from cells and cell-free membranes patches. Pflügers Arch. **391**, 85–100

13 Rauer, H. and Grissmer, S. (1996) Evidence for an internal phenylalkylamine action on the voltage-gated potassium channel $K_v$1.3. Mol. Pharmacol. **50**, 1625–1634

14 Jouirou, B., Mosbah, A., Visan, V., Grissmer, S., M'Barek, S., Fajloun, Z., Van Rietschoten, J., Devaux, C., Rochat, H., Lippens, G. et al. (2004) Cobatoxin 1 from *Centruroides noxius* scorpion venom: chemical synthesis, three-dimensional structure in solution, pharmacology and docking on $K^+$ channels. Biochem. J. **377**, 37–49

15 Fajloun, Z., Mosbah, A., Carlier, E., Mansuelle, P., Sandoz, G., Fathallah, M., di Luccio, E., Devaux, C., Rochat, H., Darbon, H. et al. (2000) Maurotoxin versus Pi1/HsTx1 toxins: Toward new insights in the understanding of their distinct disulfide bridge patterns. J. Biol. Chem. **275**, 39394–39402

16 Sabatier, J. M., Zerrouk, H., Darbon, H., Mabrouk, K., Benslimane, A., Rochat, H., Martin-Eauclaire, M.-F. and Van Rietschoten, J. (1993) P05, a new leiurotoxin I-like scorpion toxin: synthesis and structure-activity relationships of the $\alpha$-amidated analog, a ligand of $Ca^{2+}$-activated $K^+$ channels with increased affinity. Biochemistry **32**, 2763–2770

17 Romi, R., Crest, M., Gola, M., Sampieri, F., Jacquet, G., Zerrouk, H., Mansuelle, P., Sorokine, O., Van Dorsselaer, A., Rochat, H. et al. (1993) Synthesis and characterization of kaliotoxin: is the 26–32 sequence essential for potassium channel recognition? J. Biol. Chem. **268**, 26302–26309

18 Chandy, K. G., Wulff, H., Beeton, C., Pennington, M., Gutman, G. A. and Cahalan, M. D. (2004) $K^+$ channels as targets for specific immunomodulation. Trends Pharmacol. Sci. **25**, 280–289

19 Lebrun, B., Romi-Lebrun, R., Martin-Eauclaire, M.-F., Yasuda, A., Ishiguro, M., Oyama, Y., Pongs, O. and Nakajima, T. (1997) A four-disulphide-bridged toxin, with high affinity towards voltage-gated $K^+$ channels, isolated from *Heterometrus spinnifer* (Scorpionidae) venom. Biochem. J. **328**, 321–327

20 Kalman, K., Pennington, M. W., Lanigan, M. D., Nguyen, A., Rauer, H., Mahnir, V., Paschetto, K., Kem, W. R., Grissmer, S., Gutman, G. A. et al. (1998) ShK-Dap$^{22}$, a potent $K_v$1.3-specific immunosuppressive polypeptide. J. Biol. Chem. **273**, 32697–32707

21 Fajloun, Z., Carlier, E., Lecomte, C., Geib, S., di Luccio, E., Bichet, D., Mabrouk, K., Rochat, H., De Waard, M. and Sabatier, J. M. (2000) Chemical synthesis and characterization of Pi1, a scorpion toxin from *Pandinus imperator* active on $K^+$ channels. Eur. J. Biochem. **267**, 5149–5155

22 M'Barek, S., Mosbah, A., Sandoz, G., Fajloun, Z., Olamendi-Portugal, T., Rochat, H., Sampieri, F., Guijarro, J. I., Mansuelle, P., Delepierre, M. et al. (2003) Synthesis and characterization of Pi4, a scorpion toxin from *Pandinus imperator* that acts on $K^+$ channels. Eur. J. Biochem. **270**, 3583–3592

23 Batista, C. V., Gomez-Lagunas, F., Rodriguez de la Vega, R. C., Hajdu, P., Panyi, G., Gaspar, R. and Possani, L. D. (2002) Two novel toxins from the Amazonian scorpion *Tityus cambridgei* that block $K_v$1.3 and *Shaker* B $K^+$ channels with distinctly different affinities. Biochim. Biophys. Acta **1601**, 123–131

24 Possani, L. D., Selisko, B. and Gurrola, G. B. (1999) Structure and function of scorpion toxins affecting $K^+$ channels. In Perspectives in Drug Discovery and Design: Animal Toxins and Potassium Channels (Darbon, H. and Sabatier, J. M., eds.), vol. 15/16, pp. 15–40, Kluwer/Escom, Kluwer Academic Publishers, Dordrecht

25 Bardien-Kruger, S., Wulff, H., Arieff, Z., Brink, P., Chandy, K. G. and Corfield, V. (2002) Characterisation of the human voltage-gated potassium gene, KCNA7, a candidate gene for inherited cardiac disorders, and its exclusion as cause of progressive familial heart block I (PFHBI). Eur. J. Hum. Genet. **10**, 36–43

26 Koo, G. C., Blake, J. T., Talento, A., Nguyen, M., Lin, S., Sirotina, A., Shah, K., Mulvany, K., Hora, D., Cunningham, P. et al. (1997) Blockade of the voltage-gated potassium channel $K_v$1.3 inhibits immune responses *in vivo*. J. Immunol. **158**, 5120–5128

27 Beeton, C., Barbaria, J., Giraud, P., Devaux, J., Benoliel, A. M., Gola, M., Sabatier, J. M., Bernard, D., Crest, M. and Beraud, E. (2001) Selective blocking of voltage-gated $K^+$ channels improves experimental autoimmune encephalomyelitis and inhibits T cell activation. J. Immunol. **166**, 936–944

28 Beeton, C., Wulff, H., Barbaria, J., Clot-Faybesse, O., Pennington, M., Bernard, D., Cahalan, M. D., Chandy, K. G. and Beraud, E. (2001) Selective blockade of T lymphocyte $K^+$ channels ameliorates experimental encephalomyelitis, a model for multiple sclerosis. Proc. Natl. Acad. Sci. U.S.A. **98**, 13942–13947

29 Wulff, H., Calabresi, P. A., Allie, R., Yun, S., Pennington, M., Beeton, C. and Chandy, K. G. (2003) The voltage-gated $K_v$1.3 $K^+$ channel in effector memory T cells as new target for MS. J. Clin. Invest. **111**, 1703–1713

30 Panyi, G., Varga, Z. and Gaspar, R. (2004) Ion channels and lymphocyte activation. Immunol. Lett. **92**, 55–66

31 Rodriguez de la Vega, R., Merino, E., Becerril, B. and Possani, L. D. (2003) Novel interactions between $K^+$ channels and scorpion toxins. Trends Pharmacol. Sci. **24**, 222–227

32 Visan, V., Sabatier, J. M. and Grissmer, S. (2004) Block of maurotoxin and charybdotoxin on human intermediate-conductance calcium-activated potassium channels (hIKCa1). Toxicon **43**, 973–980

33 Visan, V., Fajloun, Z., Sabatier, J. M. and Grissmer, S. (2004) Mapping of maurotoxin binding sites on hKv1.2, hKv1.3 and hIKCa1 channels, Mol. Pharmacol. **66**, 1103–1112

34 Yu, K., Fu, W., Liu, H., Luo, X., Chen, K. X., Ding, J., Shen., J. and Jiang, H. (2004) Computational simulations of interactions of scorpion toxins with the voltage-gated potassium ion channel. Biophys. J. **86**, 3542–3545

35 Castle, N. A., London, D. O., Creech, C., Fajloun, Z., Stocker, J. W. and Sabatier, J. M. (2003) Maurotoxin: a potent inhibitor of intermediate conductance $Ca^{2+}$-activated potassium channels. Mol. Pharmacol. **63**, 409–418

36 Rauer, H., Lanigan, M. D., Pennington, M. W., Aiyar, J., Ghanshani, S., Cahalan, M. D., Norton, R. S. and Chandy, K. G. (2000) Structure-guided transformation of charybdotoxin yields an analog that selectively targets $Ca^{2+}$-activated over voltage-gated $K^+$ channels. J. Biol. Chem. **275**, 1201–1208

37 Mouhat, S., Mosbah, A., Visan, V., Wulff, H., Delepierre, M., Darbon, H., Grissmer, S., De Waard, M. and Sabatier, J. M. (2004) The 'functional' dyad of scorpion toxin Pi1 is not itself a prerequisite for toxin binding to the voltage-gated Kv1.2 potassium channels. Biochem. J. **377**, 25–36


Received 13 August 2004/20 September 2004; accepted 24 September 2004
Published as BJ Immediate Publication 24 September 2004, DOI 10.1042/BJ20041379